PERGAMON International Journal of Multiphase Flow 27 (2001) 1431–1449

International Journal of Multiphase Flow

www.elsevier.com/locate/ijmulflow

# Experimental study of the unsteady structure of a confined bubble plume

J. Rensen [a], V. Roig [b,*]

[a] *Department of Applied Physics, University of Twente, 7500 AE Enschede, The Netherlands*
[b] *Institut de Mécanique des Fluides, UMR CNRS 5002, Avenue Camille Soula, F-31400 Toulouse, France*

Received 18 January 2000; received in revised form 21 January 2001

**Abstract**

We present an experimental study of two-dimensional bubble plumes confined in a tank. The plumes undergo periodic oscillations. The non-stationary behaviour of the flow was studied with optical fibre probes and video camera measurements. Local void fraction and instantaneous positioning of the plume fronts were measured. For low gas flow rates, both fronts move in phase, and the geometrical centre of the plume moves in a globally periodic manner which was shown to be a progressive wave. A lot of flow configurations were observed for different gas flow rates (with or without strong interactions with the walls). A dominant periodic motion was observed even for high gas flow rates. Dependency of the oscillation frequency on the gas flow rate was measured and compared to other results from the literature. In the range of our experiments, it was observed that the water depth did not affect the structure of the plume. 

*Keywords:* Two-phase flow; Bubble plume; Experimental study; Local measurements; Unsteady state analysis

## 1. Introduction

Bubble-driven plumes are widely used in industrial plants or for environmental applications. Such applications include: gas stirring of liquid metal, aeration in wastewater treatment, destratification of reservoirs, ice prevention in lakes, and so on. Generally bubble plumes are used to stimulate liquid circulation and mixing.

The injection of bubbles into a homogeneous liquid induces entrainment of liquid from the pool and generates large-scale buoyancy-driven circulation in the surrounding liquid. The basic

* Corresponding author.
*E-mail address:* roig@imft.fr (V. Roig).

0301-9322/01/$ - see front matter 
PII: S0301-9322(01)00012-X

mechanism responsible for the creation of upward momentum of the liquid in the plume is due to buoyancy, since bubbles have a relative movement, and entrain liquid in their wakes. In the plume, the passing of different successive bubbles at a fixed point induces a mean velocity of the liquid, a sort of background constant velocity level. The passing of one distinct bubble close to a fixed point also induces, via the relative movement, a particular unsteady entrainment of liquid in the bubble wake. The liquid as a whole is thus carried upward along with the bubbles. The plume spreads by engulfing the surrounding fluid and through dispersion of the bubbles. Entrapment of exterior fluid at the plume edges is linked to entrapment by eddies that are generated by large-scale buoyancy effects or by bubble wakes (Leitch and Baines, 1989). For confined flows, recirculation of the liquid strongly influences the flow. Beneath the free surface, the entrained fluid is spread in the transverse direction, and in order to verify the continuity equation, the liquid has to flow downwards. This recirculation is influenced by nearby walls. The recirculating flow may either be steady or unsteady. In the unsteady case a global movement of the bubble plume can be observed.

In previous studies various bubble plume experiments have already been carried out. These studies concerned very large-scale bubble plumes for environmental applications (Milgram, 1983) as well as small-scale ones of a few centimetres in height for the purpose of chemical processing (Leitch and Baines, 1989; Alam and Arakeri, 1993; Becker et al., 1994; Iguchi et al., 1995; Iguchi et al., 1997; Delnoij et al., 1997). A lot of authors observed a wandering global movement of the plume (Leitch and Baines, 1989; Alam and Arakeri, 1993; Becker et al., 1994; Delnoij et al., 1997), even in large-scale experiments without strong confinement effects (Milgram, 1983). However, as far as we know, only a few experimental studies have analysed this non-stationary behaviour of bubble plumes (Becker et al., 1994; Delnoij et al., 1997). Moreover, the description of the unsteady state was limited to measuring the oscillation frequency. Generally the key problem of interest is either prediction of the liquid volume flux (Leitch and Baines, 1989; Chesters et al., 1980) or the local Eulerian description of the plume for comparison with numerical models. Concerning the prediction of liquid volume flux, Leitch and Baines have shed light on the possible great contribution of bubble wakes to liquid entrainment by observing that the entraining eddies at the edges of the flow do not simply match the scale of the centreline velocity of the liquid in bubble plume averaged over a long period of time. They also recalled the difficulty encountered in modelling fluid entrainment when there is a wandering motion of the plume. As the practical problem is always to predict the currents induced by bubble plumes in the neighbouring liquid as well as mixing, even though the wandering phenomenon is clearly important, it seemed worthwhile for us to work on characterising this unsteady movement of a confined bubble plume and to discuss the mechanisms responsible for the oscillation. Moreover, it appears that understanding bubble flows governed by gravity effects, such as the confined bubble plume, is fundamental for validating dynamic numerical models since various scales of bubble-induced movement are involved. Large-scale phenomena are mainly related to collective actions of the bubbles, and are density or buoyancy effects, while small scale phenomena are linked to bubble wake effects. Thus, this paper is an experimental study of the non-stationary behaviour of a plane vertical bubble plume, generated by air injection at the bottom of a tank. In our test conditions, we observed that this confined bubble plume wandered with a frequency of about 0.1 to 0.2 Hz.

The experimental facility, the test conditions and the measuring methods are described in Section 2. Section 3 contains the experimental results and discussion. In this study, we limited

ourselves to measurements of properties linked to the gas phase. We first introduce Eulerian measurements of the void fraction taken over a long period of time and of the velocity of bubbles. We found that our experimental results are in agreement with such locally averaged descriptions often found in the literature. We then present an analysis of time records of the positions of the plume frontiers obtained by processing video camera images. A detailed characterisation of the spatial and temporal organisation of the flow at a low gas flow rate is given. The last part of our study is an analysis of the effects of increased gas flow rate on the wandering of the plume.

## 2. Experimental set-up and measurement method

### 2.1. Experimental set-up and physical parameters governing the flow

The plane bubble plume is generated in a square tank ($150 \times 150 \times 670$ mm$^3$). The tank is filled with tap water at room temperature. The air bubbles are injected into the bottom of the tank through four rows of capillary tubes, each having 14 tubes (0.5/0.33 mm external/internal diameters) placed at intervals of 1 cm. The space between rows is also 1 cm. Consequently the width $L_i$ of the plume at the inlet is 3 cm. The length of the capillary tubes, and the pressure drop through the tubes are high enough to ensure uniform behaviour of the different injectors. A traversing mechanism, located at the top of the apparatus, allowed for displacement of the vertical intrusive probes in the three directions, across the whole apparatus. Fig. 1 shows an image of the experimental apparatus.

Parameters that might affect the behaviour of the plume are : the gas flow rate $Q_G$, the width of the plume at the inlet $L_i$, the ratio of this width to the horizontal dimension of the tank (15 cm), the water depth $H$ and the bubble diameter $d_B$. The size of the bubbles is a parameter : it is

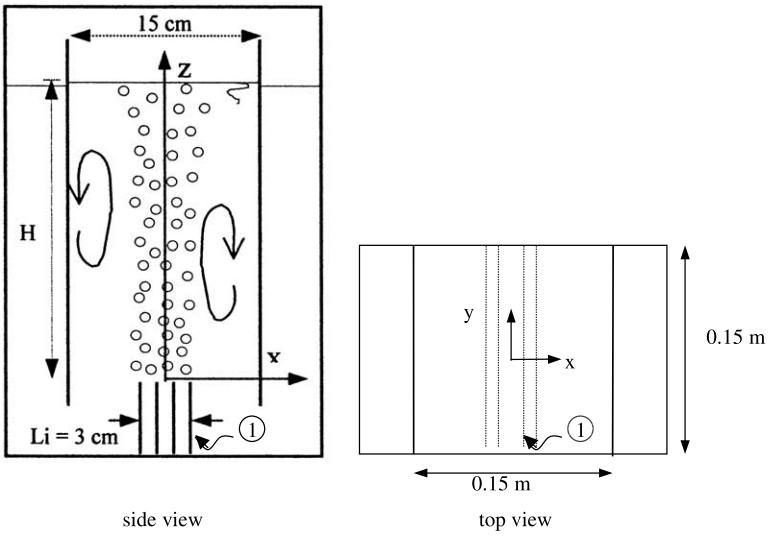


Fig. 1. Schematic diagram of the experimental set-up. (1) 4 rows of capillary tubes).

sensitive to the gas flow rate, but for each flow it is constant throughout the flow, as there is no coalescence or rupture. In this study we chose to vary the gas flow rate and the water depth. The gas flow rates $Q_G$ used were in between $1.8 \times 10^{-5}$ and $14.2 \times 10^{-5}$ $m^3/s$. The water depth $H$ was between 28 and 65 cm above the injectors. Four bubble plumes at a low gas flow rate ($2.1 \times 10^{-5}$ to $5.4 \times 10^{-5}$ $m^3/s$) were investigated in detail. Experimental conditions for each of these runs are given in Table 1.

The bubbles have an ellipsoidal form and rise in a zigzag way. Random paths of the bubbles and their wakes induce fluctuating, small scale motions in the liquid.

While it was easy to control the water depth and the gas flow rate, it was not possible to keep the bubble diameter constant for all our experiments. In fact, the bubble size just after release from the tip of the injectors is a function of the gas flow rate. Ellingsen (1998), using the same experimental configuration, measured the dependency of the bubble diameter at the nozzle of the injector upon the gas flow rate. He took measurements in the isolated bubble detachment regime existing up to $Q_G = 2.01 \times 10^{-5}$ $m^3/s$. His results are in very good agreement with the theoretical prediction of the diameter of bubbles formed at the tip of a capillary tube, made by Gaddis and Vogelpohl (1985). The bubble detachment diameter predicted by Gaddis and Vogelphol is valid in the bubbling regime up to the transition to the jetting regime where bubbles are formed by disintegration of the air jet. In our experimental conditions the injectors are at the limit of a bubbling regime. Thus in this study, in the absence of measurements for each run, we used estimates of the bubble diameter taken from Gaddis and Vogelpohl's model (see Table 1). For run $B$ the bubble size just after release was measured on a few photographs. Our estimation of the bubble equivalent diameter gave $d_B = 2.8$ mm which is in quite good agreement with both the model and with Ellingsen's measurements.

The bubble diameter is an important parameter because it determines the terminal velocity of the bubble $U_\infty$.

Without measurements it is difficult to estimate the terminal velocity of the bubbles, nevertheless this parameter is extremely important for assigning a scale to the bubble plume. The difficulty arises from the great sensitivity of the terminal velocity to experimental conditions, and thus, from the great number of experimental correlations or equations giving the terminal velocity. Using Maxworthy et al.'s (1996) experimental results, we estimated that a bubble of 2.8 mm diameter has a terminal velocity of about 26 cm/s. But Maxworthy's results were not in agreement with Ellingsen's very precise measurements for a bubble of 2.5 mm diameter as used in our set-up. Ellingsen found a terminal velocity equal to 30.4 cm/s. This velocity was in quite good agreement with the results of Duineveld (1994) who found that for a 2.68 mm diameter the terminal velocity was equal to 29.5 cm. Thus we believe that the real terminal velocity of our 2.8 mm bubbles is closer to 29.5 cm/s than to 26 cm/s. However, in the absence of measurements, the

Table 1
Experimental conditions of bubble plumes investigated in detail

| Run | *A* | *B* | *C* | *D* |
|---|---|---|---|---|
| $Q_G(10^{-5}$ $m^3/s)$ | 2.1 | 3.06 | 5.4 | 3.06 |
| H (cm) | 46.5 | 46.5 | 46.5 | 65 |
| $d_B$ (mm) Eq. (43) in Gaddis and Vogelphol | 2.8 | 3.0 | 3.4 | 3.0 |
| Camera record length (s) | 960 | 960 | 32 | 32 |

question is still open. The order of magnitude of the Reynolds number of the relative movement is thus estimated at around 700.

Some preliminary void fraction measurements were made in order to check whether the mean flow in the plume was two dimensional. The test was done for gas flow rates up to $8.6 \times 10^{-5}$ $m^3/s$ and proved to be satisfactory. Visual inspection appeared to reveal that the plume is two-dimensional at any given time, at least for its large-scale spatial behaviour.

### 2.2. Measurement methods and signal processing

An intrusive optical monofibre probe was used to make Eulerian measurements of the characteristic function of the gas phase $\chi_G$ ($\chi_G = 1$ in gas, 0 in liquid), using an RBI monofibre probe whose tip diameter was less than 50 μm. The optical fibre probe signal was converted into a two-state signal by a thresholding technique. Signal processing was then used to estimate the local void fraction $\varepsilon_G$ as well as the frequency of bubble passing, $f_b$ or the frequency of plume wandering, $f$. The error in the estimation of the time that a bubble stayed on the probe is no more important than the sampling time. For void fraction measurements a typical sampling frequency $f_e$ was equal to 2500 Hz, with the averaging time $T$ being between 400 and 800 s. Thus phase discrimination induces an error of less than 10% in the void fraction measurements.

Due to plume oscillation, the probe was sometimes in the bubble part of the plume and sometimes in the water bulk. Thus, the signal obtained by the probe at the frontier of the plume is clearly modulated. Spectral analysis of the two-state signal was performed to determine the oscillating frequency $f$. The frequency of the periodic motion of wandering of the plume was associated with the maximum in the power spectrum.

Double optical fibre probes were used to measure the mean velocity of the bubbles and to estimate the size of the bubbles captured by the probe (chords). The signal processing was based on the multichannel analysis, as described by Roig et al. (1998). The distance between both optical probes is equal to 3.1 mm.

Furthermore, since the plume is two-dimensional it is possible to detect the boundary between the bubble region and the water bulk by measuring with a video camera placed in front of the plume. We thus filmed the flow in order to analyse the spatial instantaneous structure of the frontiers of the plume. A projector and light diffusion sheets were used to illuminate the tank. The projector was placed in front of the camera. A consequence of this method is that the images show a projection of the flow on a plane. For spatial calibration we filmed a grid of known size inserted into the apparatus. Two types of video cameras were used in the experiments. One was a digital high-speed camera (EKTAPRO with a pixel resolution equal to $239 \times 192$), used at a recording rate of 50 frames per second, and with an exposure time of 1/1000 s. The other camera was an ordinary video camera with a recording rate of 25 frames per second and a greater exposure time (1/50 s). The resolution of this camera is $500 \times 582$ pixels. The ordinary video camera was used because the maximal recording length of the high-speed camera was limited to 1600 images, which was not sufficient. The results of the high-speed camera were interesting because the images showed greater contrast between the bubbles and the water bulk than the images obtained by the ordinary camera. This was due to the difference in exposure time of the two cameras.

Image processing software had to be developed. For the high-speed camera the time lapse between two digitised frames was set at 0.4 s. For the ordinary camera an image was acquired

every 0.6 s. After digitising, a background correction was carried out. This consisted of dividing the luminance values of an image by the luminance values of a background image. Then, we converted the images into binary images by means of a threshold value method. The threshold was determined by trial and error. The result was a binary black and white image where the bubbles appeared in black. The original image was compared to the binary image, to check that the chosen threshold value was correct (e.g. Fig. 2). At the bottom of the binary image, one can still see the injectors which do not disappear completely because the background image is taken with the tank filled with air instead of water. The reason is that it is not possible to stop injecting air if the gas flow rate is to be kept under control and stable.

The binary images are used to obtain the position of the boundary between the outer flow and the bubble region. The positions $A(z,t)$ and $B(z,t)$ in the projection on the $(x,z)$ plane of the extreme bubbles at a certain height are taken as the positions of the two boundaries of the plume at that height. The flow region affected by the plume is certainly larger than the flow region containing bubbles (Milgram, 1983). However, this arbitrary definition is clear and easy to adopt and will still be useful for quantitative comparison with numerical work.

The position of the boundary is detected as follows. The luminance values of an image are read on horizontal lines placed at intervals equal to 2 mm. The width of the line is equal to a pixel. The lines are divided into sampling units whose length is about 1 mm. If no bubbles are found in a

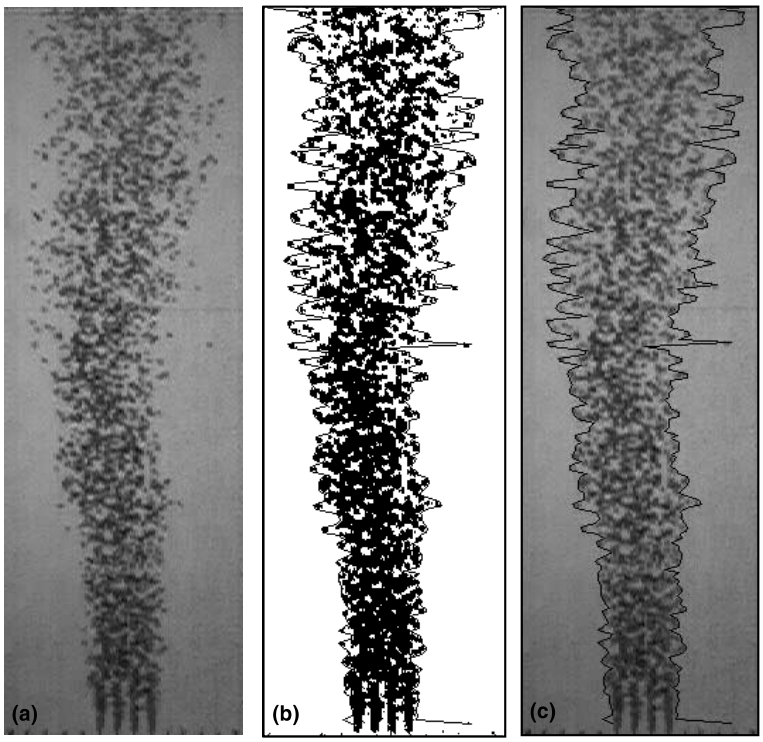


Fig. 2. Treatment of an image: (a) original image, (b) binary image, (c) original image and boundaries. $Q_g = 3.06 \times 10^{-5}$ m$^3$s$^{-1}$, image size 38 × 15 cm.

sampling unit then the mean luminance value corresponds to white. Whenever a bubble is found in a sampling unit the luminance value deviates from the luminance value for white. Thus the position of the extreme bubbles on a line is measured by detecting the first and last sampling units which have a luminance value different from white.

Fig. 2 shows different stages of the treatment of an image obtained by the high-speed camera: an original image, the corresponding binary image and once again the original image with boundaries as detected. In the last two images the found boundaries are superposed. The images show that the procedure to determine the boundary gives satisfactory results.

The accuracy of the measurement method and of the image processing was tested by comparing frontier positions obtained independently with the high-speed camera and the ordinary camera for the same flow (run $B$). The mean positions of the frontiers proved to be the same with a maximum accuracy error of 2 mm.

Instead of analysing the movements of both the $A$ and $B$ frontiers we will analyse

$$X_C = \frac{A+B}{2} \quad \text{and} \quad L = A - B,$$

where $X_C$ is the geometrical centre of the plume and $L$ is the width of the plume. As we do not know if the instantaneous gas distribution is symmetrical inside the plume, we cannot ascertain whether $X_C$ represents the centre of gravity of the plume or not.

## 3. Experimental results and discussion

We first report long-time average measurements. Such measurements have often been discussed by previous authors. However our results are still interesting as most of the reported experimental studies described round bubble plumes and not plane ones. On the other hand, our bubble plumes have an unstable asymmetrical topology. They wander at a low frequency (from 0.1 to 0.2 Hz). Accordingly, measurements averaged over a long period of time do not allow for a clear dynamic description of the plume. Consequently analysis of the non-stationary behaviour is then discussed.

### *3.1. Average description of the plume*

At a low gas flow rate, a mean description of the flow was obtained using Eulerian measurements averaged over a long period of time. We made a detailed investigation of plume $B$.

From the void fraction profiles (Fig. 3), the general mean behaviour of the plume can be determined. The mean plume is symmetrical with respect to the vertical $(y,z)$ plane. The centreline value of the void fraction decreases gradually in the longitudinal direction, and the width of the plume increases. Both tendencies result from the combined effects of the bubble dispersion and of the plume wandering. In this experimental approach it is not possible to separate the two effects. Generally in bubble plume studies, void fraction profiles are plotted against self-similar co-ordinates, and self-preserving profiles may be successfully compared to Gaussian curves (Iguchi et al., 1995). In our experimental conditions, in which a strong wandering was detected, at a certain distance from the inlet, void fraction profiles are still in quite good agreement with Gaussian

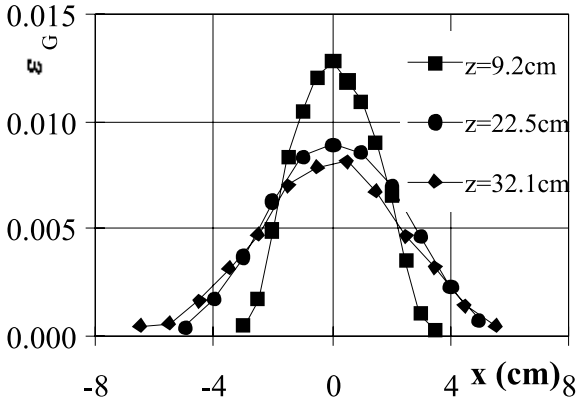


Fig. 3. Void fraction profiles in plume $B$ at various longitudinal positions.

curves. But this plotting is not pertinent in order to make a clear distinction between dispersive effects and bubble transport by the wandering.

The bubble passage frequency $f_b$ has also been estimated (Fig. 4). The profiles show the same tendencies as the void fraction profiles. It is interesting to notice that the bubble frequency is not at all representative of the frequency of the intermittent movement of the plume which is about 0.1 Hz. The wandering of the plume cannot therefore be a response to the detachment of the bubbles near the injection system.

The liquid velocity was not measured. However rising bubbles entrain liquid and, as a result, a liquid flow is generated. In Fig. 5 we show some measurements of the mean velocity of the bubbles $U_G$. The profiles are very flat, and the average gas velocity is about 0.42 m/s. The uncertainties in measurements of gas velocity are however quite high (20%) due to the wandering motion of the bubbles. The liquid velocity in the plume is thus estimated to be about 10 or 15 cm/s, calculated as the difference between the measured value of the bubble mean velocity and the terminal rise velocity of bubbles with a diameter of 2.8 mm. Such a flat gas velocity profile is quite surprising. Bubble mean vertical movements are uniform in the $x$ direction. Inside the bubbly core of the

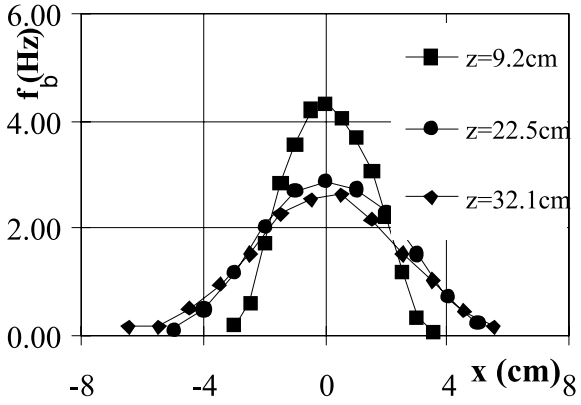


Fig. 4. Frequency of bubble passages $f_b$ in plume $B$ at various longitudinal positions.

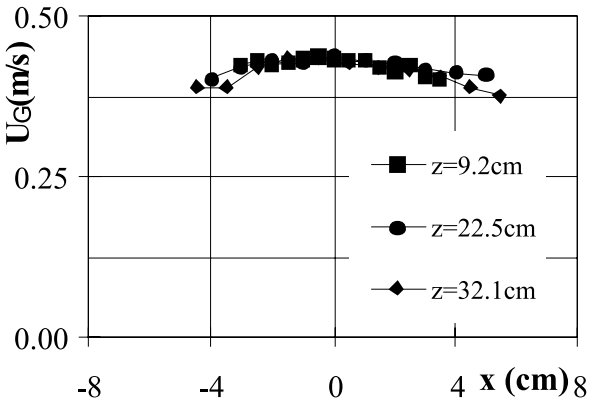


Fig. 5. Mean velocity of bubbles in plume $B$ at various longitudinal positions.

plume, the liquid phase has quite a uniform vertical velocity that does not change with height when far enough away from the nozzles. The absence of any longitudinal evolution in the centerline value of bubble velocity $U_{GC}$ is in agreement with the self-preserving theoretical predictions made in two-dimensional plumes driven by a line source of heat (Tennekes and Lumley, 1972). Thus, such a self-preserving analysis based on a comparison with thermal effects correctly predicts that this scale is constant over the whole flow. However, it cannot explain the absence of any transverse variation. In our experimental conditions self-preservation analysis is irrelevant because of confinement and wandering effects.

Observation of the bubble formation at the end of the injectors shows that bubble diameter is quite constant. The mean bubble chord $l_x$ seen by the double optical fibre probe is equal to 1.4 mm. It is constant across the whole flow. We have not converted the mean chord into a mean bubble diameter. Even if the shape of the bubbles is known – it is an ellipsoid – the relationship between size distribution and chord length distribution is not easy to model because of the zigzag trajectories of the bubbles and of random piercing. Existing theoretical models (Clark and Turton, 1988) do not apply in our case because they do not take into account the changes in the orientations of ellipsoids.

### 3.2. Study of the non-stationary behaviour of the plume

Four bubble plumes that we have explored in detail with a camera were characterised by quite low gas flow rates. These four runs will first be discussed. For the other runs ($Q_G > 5.4 \times 10^{-5}$ m$^3$s$^{-1}$) we will then give a shorter analysis of the sensitivity of the flows to the gas flow rate. The distinction between the cases at "low" and "high" gas flow rates is based on the experimental observation of the absence of phase shift between both frontiers of the cases at "low" gas flow rates.

#### 3.2.1. Bubble plumes at low gas flow rates ($Q_G < 5.4 \times 10^{-5} m^3 s^{-1}$)

*3.2.1.1. Nature of the oscillatory movement of the plume*. For low gas flow rates, the two frontiers of the plume move with a sinuous oscillation and are in phase. Interspectral analysis was

performed for long records (runs *A* and *B*). It showed that the phase shift between frontiers *A* and *B* is equal to zero.

While the central position of the plume oscillates with a clear dominant frequency (see Fig. 6), the records of the width of the plume show that this variable is noisier (Fig. 6). The comparison of the spectra of $X_C$ and of $L$ (Fig. 7) reveals the periodic component of the motion of $X_C$ with a frequency of 0.104 Hz, and the absence of any dominant frequency in the signal of $L$ for run *B*. Thus there is no various oscillation mode.

The observation of the asymmetric oscillation agrees with previous related observations in confined as well as unconfined bubble plumes (Becker et al., 1994; Delnoij et al., 1997; Milgram, 1983). Pera and Gebhart (1971) have shown through numerical simulations that laminar thermal plumes arising from a hot horizontal line are less stable for asymmetric disturbances than for symmetric ones. In experiments in air they found a predominant asymmetric mode of flow oscillation. Observations of transitions in plane laminar bubble plumes were made by Alam and

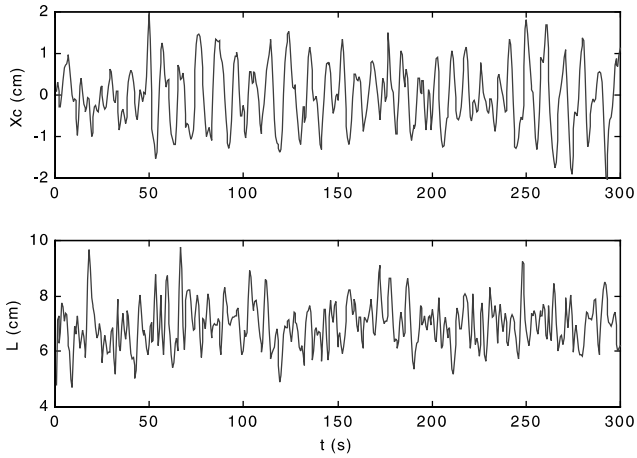


Fig. 6. Records of the movement of the geometrical centre of the plume $X_C$ and – of the width of the plume $L$ at $z = 20$ cm. (Plume *B*).

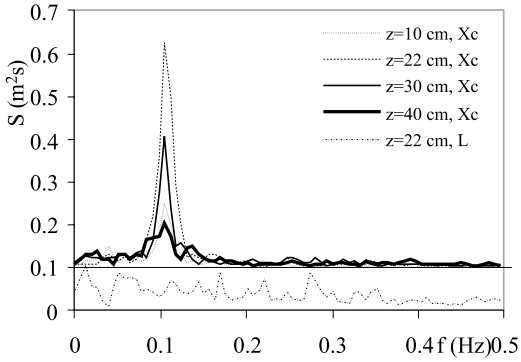


Fig. 7. Spectra of the geometrical centre of the plume $X_C$ and of the width of the plume $L$ at different $z$ positions in plume *B*. (Spectra of $X_C$ have been shifted by 0.1 $m^2$ s to visualise details).

Arakeri (1993). In their experiments the gas flow rates were very low in comparison to ours, and the slip velocity of the bubbles was about 1 cm/s. They also observed an intrinsic sinuous mode of instability with a meandering path.

At low gas flow rates, we observed that the dominant frequency of the oscillating movement of the centre does not evolve significantly in the flow. The spectra of $X_C$ at several downstream positions clearly show that the maximum of the spectra are always located at the same frequency (Fig. 7). It is clear that the horizontal density gradient of the fluid mixture on the one hand, and the velocity profile of the liquid entrained by bubbles on the other hand, are the driving terms of the unstable behaviour of our bubbly plume. However the wall effects or the confinement may influence the selection of the frequency of the wandering of the plume.

Since the water depth was high enough, the free surface did not show periodical oscillations. Therefore it is not to be expected that the free surface influences or is coupled with the oscillating frequency of the plume in the flow regimes observed. On the other hand, the random helicoïdal movements of the bubbles cannot excite the global oscillating movement, since they are not energetic enough, and the frequency of a helicoïdal path is very different from the frequency of the global sinuous movement (Ellingsen and Risso, 1998).

A cross-correlation analysis was done between records of $X_C$ at measuring positions separated in the longitudinal direction. This was used to determine the phase shift in the longitudinal direction associated with the dominant frequency. For low gas flow rates the phase shift was found to be linear with $z$ for $5 < z < 35$ cm (Fig. 8). At the bottom and top of the tank, the phase shift was very noisy and it is not possible to draw any conclusions. The linear shift proves that $X_C$ behaves like a progressive wave. The wave velocities $u_w$ associated with runs $A$ and $B$ are given in Table 2. Phase shift results obtained in plume $B$ with the ordinary camera are confirmed by a fitting analysis of a short record taken in the same experimental conditions with the Ektapro camera (result denoted $B'$ in Table 2). The associated wavelength $\lambda_w$ is also given in this table. The progressive wave-like behaviour is probably due to an interaction of the bubble plume with vortices that are formed at the top of the tank, and that travel downwards in a staggered vortices flow pattern. Several experimental or numerical studies of bubbly plumes have discussed the link between the movements of the vortices and wandering of the plume (Delnoij et al., 1997; Becker et al., 1994; Mudde and Simonin, 1999; Ayukawa et al., 1998). More recently Delnoij et al. (1999) have visualised large vortices at the frontier of a bubble plume using PIV methods. In our

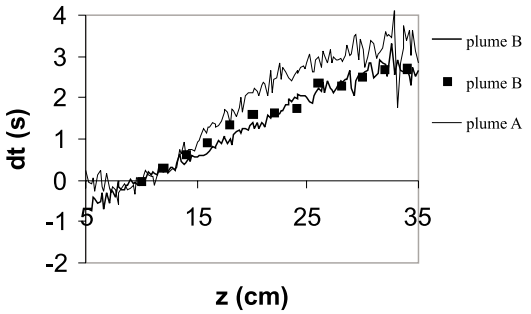


Fig. 8. Longitudinal phase shift of the wavy motion. (continuous lines: results obtained from ordinary camera records; points: results obtained from Ektapro camera records) $dt = \Delta\varphi/2\pi f$.

Table 2
Experimental results

| Run | *A* | *B* | *B′* | *D* |
|---|---|---|---|---|
| $f$ (Hz) | 0.094 | 0.104 | 0.104 | 0.104 |
| $u_w$ (cm/s) | 4.9 | 7.1 | 7.5 | 7.8 |
| $\lambda_w$ (cm) | 52 | 68 | 72 | 75 |

experiment some preliminary visualisations of the liquid phase movements, obtained with laser sheet light, showed vortices aligned with the $y$ axis on each side of the plume. Some travel vertically from top to bottom. We have made a crude estimation of the frequency with which vortices pass a given station $z$. This frequency is similar to the frequency of the plume wandering. Thus the selection of the frequency of wandering is strongly related to the global coupling of the bubble plume with the external flow.

The value of the wave velocity increases with $Q_G$. This is consistent with the idea that vortices velocity is related to the velocity of the liquid induced inside the plume. The same trend was observed at the transition of laminar bubble plumes (Alam and Arakeri, 1993). In our case, the wavelength also increased with $Q_G$. This trend has not been observed for laminar bubble plumes (Alam and Arakeri, 1993) or for buoyant plumes (Kimura and Bejan, 1983). It is believed that it is an effect of the present confinement, as such a behaviour is observed in the wandering regimes in bubble columns (Lin et al., 1996).

*3.2.1.2. Amplitude of the oscillatory movement*. The movement of the geometrical centre of the plume appears to be sinusoidal with a fixed frequency, and a random amplitude. Instantaneous frequency analysis using Hilbert transformation confirms that the dominant frequency of $X_C$ is quite time-independent, even if the instantaneous amplitude is noisy. This movement of $X_C$ is centred on the $0z$ axis because the flow is symmetrical with respect to the vertical direction. The time records of the geometrical centre of the plume at several longitudinal positions show that the RMS value of the movement of the centre increases in the downstream direction, at least up to $z = 20$ cm. The RMS values of $X_C$ are reported for two gas flow rates in Fig. 9. Effects of the walls are present and may explain the saturation observed above $z = 20$ cm. The probability density function of $X_C$ (Fig. 10) is not that of a pure sinus because noise is added to the sinus phenom-

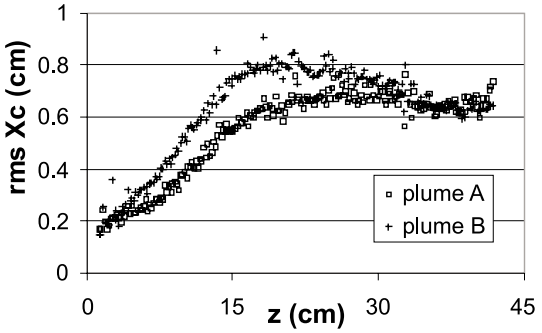


Fig. 9. Amplitude of the oscillations: RMS value of the centre position $X_C$ (Plumes *A* and *B*).

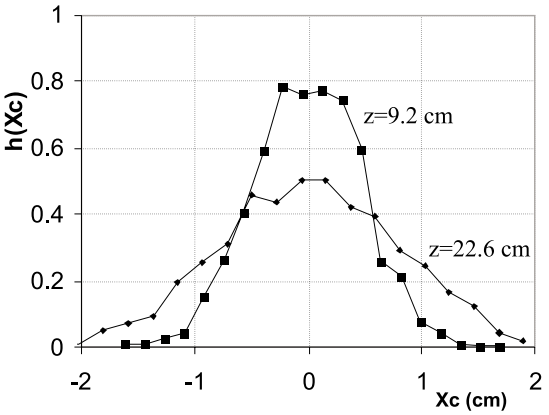


Fig. 10. Probability density function of the centre position $X_C$: $h(X_C)$ (Plume $B$).

enon. The noise seems to be of a white noise type as can be deduced from the spectral analysis (see Fig. 7 for example). This noise is linked to the dispersion of the bubbles at the frontiers of the plume, but is not simply related to the local dispersion phenomenon, since we are dealing with images averaged in one direction. If the noise is assumed to be independent of the sinuous movement, the probability density function of $X_C$ thus results from the convolution of the density of a pure sinus and of a Gaussian probability density function associated with the noise. For a low signal-to-noise ratio, the resulting probability density function is essentially of the Gaussian type. Thus, due to the noise, we can only say the amplitude of the sinuous movement of the centre of the plume is less than $\sqrt{2\overline{x'^2_C}}$.

*3.2.1.3. Width of the plume*. The variation in the width of the plume $L$, at a certain height, is random and appears to be noisier than $X_C$ (see Fig. 6).

In Fig. 11, the longitudinal evolution of the mean width $\bar{L}$ is reported for several gas flow rates. The width of the plume increases in the longitudinal direction. The plume expansion is due to bubble transverse dispersion. When the gas flow rate increases, the spreading rate is increased due to a stronger dispersion of the bubbles.

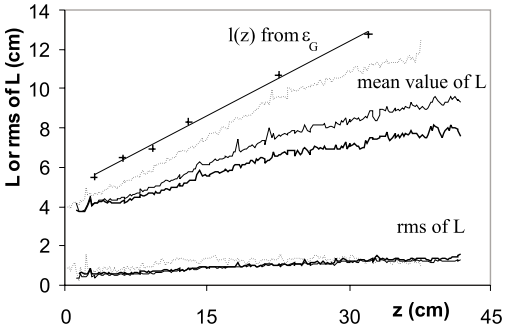


Fig. 11. Width of the plumes Mean and rms values of $L(z)$ defined from image analysis: ▬ plume $A$, —— plume $B$, - - - plume $C$ Mean width $l(z)$ defined from void fraction profiles in plume $B$: +.

The RMS value of $L$, denoted $\sqrt{\overline{L'^2}}$, is low, not very sensitive to the gas flow rate, and does not evolve significantly in the downstream direction (Fig. 11). The RMS value of $L$ results from the random helicoïdal trajectories of the bubbles. All along the plume, visualisations show that the intrinsic helicoïdal movement of the bubbles persists. The RMS value of $L$ is quite equal to the order of magnitude of the amplitude of the helicoïdal trajectories of isolated bubbles of similar size measured by Ellingsen and Risso (1998).

Then $L(z)$ is compared with the width $l(z)$ estimated from gas hold-up measurements with the optical fibre probe (Fig. 11). The width $l(z)$ was defined as the distance between the frontiers of void fraction profiles (intersection between extrapolated profile and axis $\varepsilon_G = 0$). It is worth noting that the difference between both length scales is very important. When a spreading rate is estimated from optical fibre probe measurements, it is therefore strongly overestimated due to sinuous large-scale movement. The plume is in fact more concentrated than when detected by Eulerian measurements. Eulerian measurements thus introduce a bias in the definition of a precise diffusive scale. We have made a quantitative estimation of this bias due to non-stationary large-scale motions. The ratio $\bar{L}(z)/l(z)$ evolves downstream because the ratio of $\bar{L}$ to $\sqrt{\overline{x_C'^2}}$ evolves, but $\bar{L}(z)/l(z)$ is about 0.7–0.8. In order to describe such a confined bubble plume, it is thus important to take the time-dependent behaviour of the flow into account.

### 3.2.2. *Influence of the increase in the gas flow rate*

*3.2.2.1. Qualitative description of various flow regimes.* While at the lowest gas flow rates, the phase shift between both frontiers is equal to zero, thus allowing for a simple analysis of the global movement of the plume, at higher gas flow rates the dynamic behaviour of the plume is more complicated.

Depending on $Q_G$, several non-stationary phenomena of bubble plume behaviour may be observed as shown in Fig. 12. In this figure, several sequences of successive binary images at various values of $Q_G$ are shown. Whatever the gas flow rate, we observed an oscillating movement of the flow. At low $Q_G$ (Fig. 12(a)) we observed, in addition to a small dispersion of the bubbles in the transverse direction and a low increase of the plume diameter in the longitudinal direction, the large-scale sinuous wandering of the plume. In this low gas flow rate configuration, bubble collisions with the walls are confined to the upper part of the plume. When increasing the gas flow rate, spatial and temporal characteristics of the plume evolve. Fig. 12(b) and (c) show that the spreading rate of the plume increases with an increased gas flow rate. For bubble plumes at higher gas flow rates, a phase shift was observed between both frontiers (Fig. 12(b)). The width of the plume is modulated. For higher gas flow rates, the movements of the frontiers are more complicated even if a dominant oscillation persists (Fig. 12(c)). The interactions with the wall then become stronger (the number of bubbles that collide with the walls increases with $Q_G$, and the minimal height at which collisions with the walls may appear decreases). The movement of the plume becomes more violent for high $Q_G$. In the last image a cluster of bubbles is travelling downwards, probably due to transport in a strong descending vortex.

*3.2.2.2. Persistence of a dominant frequency.* A study of the spectrum of the characteristic function of the gas phase obtained by the optical probe shows that it evolves with the gas flow rate (Fig. 13).

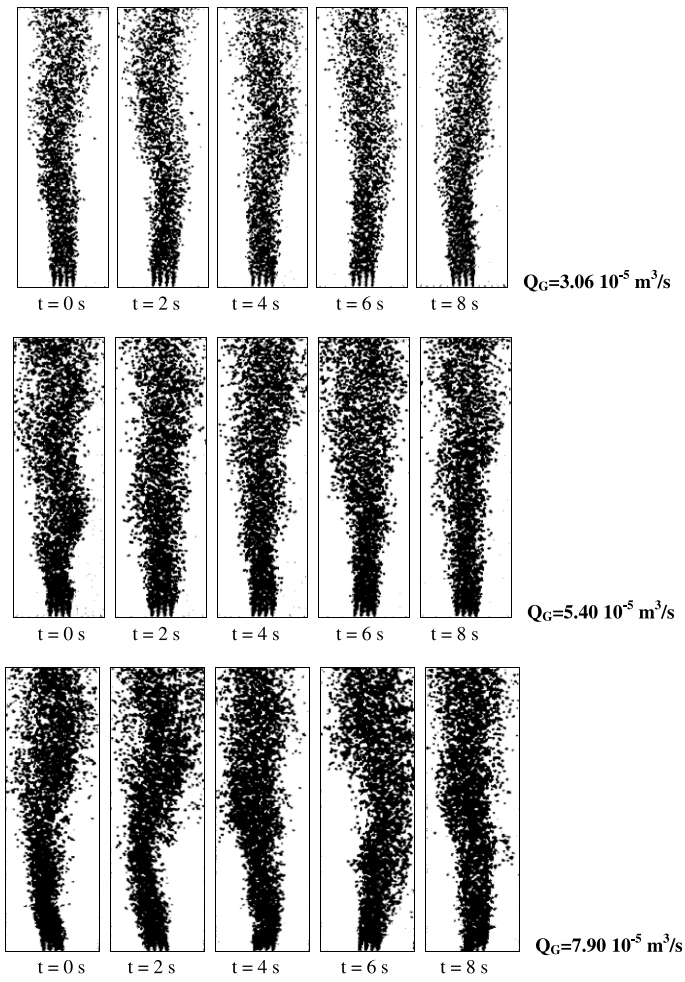


Fig. 12. Images of various bubble plumes after binary conversion at various instants. $H = 46$ cm. Size of the images: $38 \times 15$ cm$^2$.

The frequency $f$ of the plume wandering is the dominant frequency in this spectrum. When the gas flow rate was increased we observed that the peak of the spectrum was increased and shifted to higher frequencies. While increasing $Q_G$ we always observed a single dominant frequency. The plume has a strong persistent global periodic movement. The bubble dispersion influences the noise of the spectrum. It is quite similar to white noise, and its level also increases with the gas flow rate.

In Fig. 14 we have reported the frequency of wandering as a function of the gas flow rate injected at the inlet of the plume for all the runs.

### *3.2.3. Influence of the water depth H*

The water height above the injectors was varied between 27.7 and 65 cm. The frequency of wandering was found to be independent of this water height (see Fig. 14). In their experimental

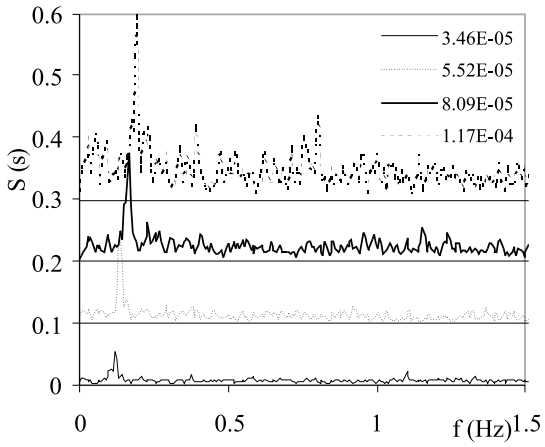


Fig. 13. Spectra of optical fibber probe records at different gas flow rates. ($Q_G = 3.46 \times 10^{-5}$, $5.52 \times 10^{-5}$, $8.09 \times 10^{-5}$ and $1.17 \times 10^{-5}$ $m^3/s$). (Each graph has been shifted by 0.1 s to visualise details).

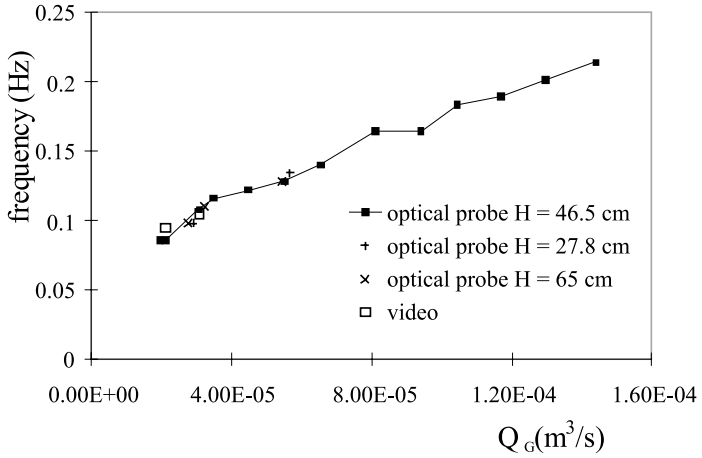


Fig. 14. Frequency of the wandering motion $f$ as a function of the gas flow rate $Q_G$.

measurements, Delnoij et al. (1997) have found that the oscillation frequency of confined bubble plumes is a function of the aspect ratio $H/W$, where $W$ is the width of the tank (15 cm in the present work). They found that an effect of this ratio exists only when the ratio is lower than 2 or 3. In our experiments the frequency was found to be independent of the aspect ratio when $H/W$ was varied between 1.8 and 4.3. Thus our results are consistent with those of Delnoij et al.

Moreover, for plume $D$ we observed that the longitudinal profiles of $\bar{L}$, $\sqrt{\overline{L'^2}}$ and $\sqrt{\overline{x'2_C}}$ are identical to those of plume $B$. The value of the wave velocity of plume $D$ was also obtained by fitting the short records to a sinusoidal function (see Table 2). The wave velocity is identical to the one obtained with the same gas flow rate, and a lower water depth in plume $B$. Thus, given the range of our experiments, we can expect the wave velocity to be independent of the water depth.

*3.2.4. Comparison with other experiments*

It is interesting to normalise our results in order to compare them with those of Delnoij et al. (1997) and Becker et al. (1994). These authors studied the frequency of wandering of bubble plumes in water with bubble diameters, gas velocity and geometrical conditions quite similar to ours. Non-dimensional analysis starts with the list of physical parameters governing the movement of the plume with $g$ being the acceleration due to gravity, $L_\mathrm{i}$ the width of the injection, $\rho_\mathrm{L}$ the density of the liquid, $v$ the kinematic viscosity of the liquid, $U_\mathrm{GS}$ the superficial velocity of the gas, and $U_\infty$ the terminal velocity of the bubbles. $U_\mathrm{GS}$ is an important parameter because it determines the difference of density between the plume and the pure liquid which controls the buoyancy-induced motions. The surface tension is not included in the non-dimensional analysis because its effects are not important in the present experiment: the size of the bubbles is determined by the inlet conditions. We did not introduce $d_\mathrm{B}$ the mean diameter of the bubbles as a parameter as we believe that its effect is to fix the slip velocity. The density of the gas is not taken into account, because it is negligible compared to the density of the liquid. The aspect ratio is not introduced because it has no effects in the range of our experiments. Thus the functional relationship between the frequency of wandering of the plume $f$ and the various parameters can be written as $F(f, g, L_i, \rho_\mathrm{L}, v, U_{GS}, U_\infty) = 0$. We can formulate the following four independent non-dimensional numbers that govern the behaviour of the flow as:

- A normalised frequency, a sort of Strouhal number: $f^* = fL_\mathrm{i}/U_\mathrm{GS}$.
- An equivalent Prandtl number: $Pr = v/U_\infty L_\mathrm{i}$.
- A Froude number: $Fr = U_\infty/gL_\mathrm{i}$.
- A Rayleigh number defined as in Kimura and Iga (1995): $Ra = gL_\mathrm{i}^2 U_\mathrm{GS}/vU_\infty^2$ .

The Prandtl number and the Froude number are quite similar in those experiments, so it is not possible to discuss their influence. Given the lack of more precise information we used a terminal velocity equal to 0.3 m/s in all studies in order to normalise the results. Our results are in good agreement with those of Delnoij et al. when $f^*$ is plotted against the equivalent Rayleigh number (Fig. 15). Agreement is less clear with the results of Becker et al. (1994)

Kimura and Iga (1995) studied the convective flows produced by the buoyancy of small bubbles rising from the horizontal bottom of a thin water layer. They discussed the possible comparisons between convective motions induced by bubbles and thermal convection. They used a system of

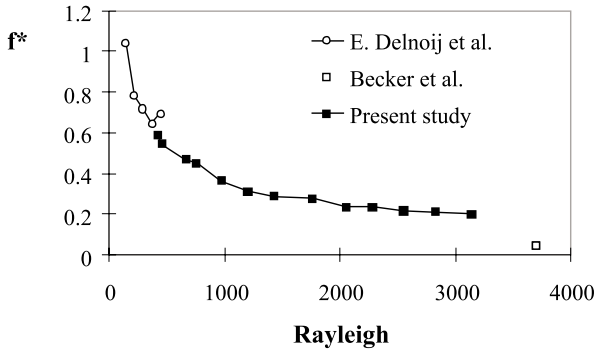


Fig. 15. Comparison of non-dimensional frequency with other results.

transport equations which is identical to that of thermal free convection under Boussinesq's approximation, except that temperature perturbation is replaced by void fraction which is advected by the bubble velocity instead of being diffused according to the Fickian thermal diffusion law. The scaling of this system of equation of course leads to the same non-dimensional numbers as in our previous global non-dimensional analysis. The correspondence between our non-dimensional results and those of Delnoij et al., thus reveals that this analysis is relevant in these bubble plumes. This is because both are controlled by gravity effects, and also by integral effects of buoyancy, i.e., average density variations.

## 4. Conclusion

In buoyancy-driven unsteady bubbly flows there can be strong interactions between phenomena at different time and space scales. Our unsteady description of the flow will thus be useful for the validation of dynamic models where the full unsteady hydrodynamics of the convective and dispersive transport processes are analysed. In our experiments, the unsteadiness is of fundamental importance because the bubble plumes presented an oscillatory movement no matter what the gas flow rate. At low gas flow rates, the large-scale motion of the plume has a global periodical nature which looks like a progressive wave. The confinement effects were found to determine the value of the frequency of the oscillation. At higher gas flow rates, even if the bubbles do strongly interact with the recirculating flow, a dominant frequency remains which is characteristic of the global motion of the plume. Non-dimensional analysis and comparison with other experimental results revealed that large-scale oscillations of confined bubble plumes are mainly controlled by buoyancy.

## References

Alam, M., Arakeri, V.H., 1993. Observations on transition in plane bubble plumes. J. Fluid Mech. 254, 363–374.

Ayukawa, K., Morinaga, E., Ochi J., Kawahara, G., 1998. Numerical investigation of symmetry breakdown in the flow induced by rising small bubbles. In: Third International Conference on Multiphase Flows, ICMF'98, Lyon, France, 8–12 June.

Becker, S., Sokolichin, A., Eigenberger, G., 1994. Gas–liquid flow in bubble columns and loop reactors: Part II. Comparison of detailed experiments and flow simulations. Chem. Eng. Sci. 49, 5747–5762.

Chesters, A.K., van Doorn, M., Goossens, L.H.J., 1980. A general model for unconfined bubble plumes from extended sources. Int. J. Multiphase Flow 6, 499–521.

Clark, N.N., Turton, R., 1988. Chord length distributions related to bubble size distributions in multiphase flows. Int. J. Multiphase Flow 14, 413–424.

Delnoij, E., Kuipers, J.A.M., Swaaij, W.P.M., 1997. Dynamic simulation of gas–liquid two-phase flow: effect of column aspect ratio on the flow structure. Chem. Eng. Sci. 52, 3759–3772.

Delnoij, E., Westerweel, J., Deen, N.G., Kuipers, J.A.M., Swaaij, W.P.M., 1999. Ensemble correlation PIV applied to bubble plumes rising in a bubble column. Chem. Eng. Sci. 54, 5159–5171.

Duineveld, P.C., 1994. Bouncing and coalescence of two bubbles in water. Ph.D. thesis, Universiteit Twente, The Netherlands.

Ellingsen, K., Risso, F., 1998. Measurements of the flow field induced by the motion of a single bubble. In: Third International Conference On Multiphase Flow, ICMF'98, Lyon, France, 8–12 June 1998.

Ellingsen, K., 1998. Hydrodynamique des écoulements pilotés par l'ascension de bulles d'air virevoltantes. Ph.D. thesis, Institut National Polytechnique de Toulouse, France.

Gaddis, E.S., Vogelpohl, A., 1985. Bubble formation in quiescent liquids under constant flow conditions. Chem. Eng. Sci. 41, 97–105.

Iguchi, M., Ueda, H., Uemura, T., 1995. Bubble and liquid flow characteristics in a vertical bubbling jet. Int. J. Multiphase Flow 21, 861–873.

Iguchi, M., Okita, K., Nakatani, T., Kasai, N., 1997. Structure of turbulent round bubbling jet generated by premixed gas and liquid injection. Int. J. Multiphase Flow 23, 249–262.

Kimura, R., Iga, K., 1995. Bubble convection. In: Redondo, Métais (Eds.), Mixing in Geophysical Flows, CIMNE, Barcelone, pp. 34–51.

Kimura, S., Bejan, A., 1983. Mechanism for transition to turbulence in buoyant plume flow. Int. J. Heat Transfer 26, 1515–1532.

Leitch, A.M., Baines, W.D., 1989. Liquid volume flux in a weak bubble plume. J. Fluid Mech. 205, 77–98.

Lin, T.J., Reese, J., Hong, T., Fan, L.S., 1996. Quantitative analysis and computation of two-dimensional bubble columns. AIChE J. 42, 301–318.

Maxworthy, T., Gnann, C., Kürten, M., Durst, F., 1996. experiments on the rise of air bubbles in clean viscous liquids. J. Fluid Mech. 321, 421–441.

Milgram J.H, 1983. Mean flow in round bubble plumes. J. Fluid Mech. 133, 345–376.

Mudde, R.F., Simonin, O., 1999. Two- and three-dimensional simulations of a bubble plume using a two-fluid model. Chem. Eng. Sci. 54, 5061–5069ss.

Pera, L., Gebhart, B., 1971. On the stability of laminar plumes: some numerical solutions and experiments. Int. J. Heat Mass Transfer 14, 975–984.

Roig, V., Suzanne, C., Masbernat, L., 1998. Experimental investigation of a turbulent bubbly mixing layer. Int. J. Multiphase Flow 24, 35–54.

Tennekes, H., Lumley, J.L., 1972. A First Course in Turbulence. MIT Press, Cambridge, MA.